# General phase-diagram of multimodal ordered and disordered lasers in closed and open cavities

F. Antenucci[1,2], C.Conti[1,3], A. Crisanti[1,3] and L. Leuzzi[2,1*]
[1] *Dipartimento di Fisica, Università di Roma "Sapienza," Piazzale A. Moro 2, I-00185, Roma, Italy*
[2] *IPCF-CNR, UOS* Kerberos *Roma, Piazzale A. Moro 2, I-00185, Roma, Italy*
[3] *ISC-CNR, UOS* Sapienza*, Piazzale A. Moro 2, I-00185, Roma, Italy*

We present a unified approach to the theory of multimodal laser cavities including a variable amount of structural disorder. A general mean-field theory is studied for waves in media with variable non-linearity and randomness. Phase diagrams are reported in terms of optical power, degree of disorder and degree of non-linearity, tuning between closed and open cavity scenario's. In the thermodynamic limit of infinitely many modes the theory predicts four distinct regimes: a continuous wave behavior for low power, a standard mode-locking laser regime for high power and weak disorder, a random laser for high pumped power and large disorder and an intermediate regime of phase locking occurring in presence of disorder below the lasing threshold.

arXiv:1406.7826v1 [physics.optics] 30 Jun 2014

In describing cavity-less lasers with randomly placed scatterers, generically called random lasers (RLs) [1–11], the most challenging issue is the interplay between disorder and non-linearity. In RLs the lasing is due to stimulated amplification of light spatially localized in leaky stochastic resonators [1]. If disorder is dominant and non-linearity negligible, stimulated amplification of light can be hindered because of diffusion. Conversely, if the structural disorder is weak, the effect on nonlinear evolution is marginal and does not modify the standard laser features. Competition occurs when wave scattering affects the degree of localization and non-linearity couples the localized modes. Various recent experimental results show that the coupling between modes changes the degree of spatial localization and their spatial and spectral correlations [12–14].

In this Letter, we report a theoretical analysis comprehensively describing all the possible regimes, accounting for the fact that light modes exhibit a distribution of localization lengths, and an interaction determined by the overall energy. In a general statistical mechanical framework, we predict specific transitions from incoherent to coherent regimes, both in the case of standard mode-locking lasers in a closed cavity and for cavity-less disordered systems with strong gain. The latter displaying a *glassy* coherent behavior. We also define and consider, as an independent parameter, a *degree of non-linearity*. As *glassy* we mean that (i) a sub-set of modes out of an extensive ensemble of localized passive modes are activated in a non-deterministic way [40] and (ii) the whole set of activated modes behaves cooperatively and belongs to one state out of many possible ones. The system properties can be represented by a corrugated landscape composed of many valleys separated by high mountains and hidden passes. The overall coherence arises from the trapping in a metastable state in the landscape.

We identify four different equilibrium phases: continuous wave (CW$\sim$), phase-locked wave (PLW$\natural$), standard ML laser (SML$\|$), random lasing (RL$\star$). In previous work, phases of modes were retained as the only relevant dynamic variables [9, 15]. Here we remove this *quenched amplitude* approximation and provide a general picture of all the regimes attainable in a multi-modal laser at any degree of pumping, disorder, and cavity leakage.

*The complex amplitude model.* — For a closed cavity, localized modes form a complete set and the electromagnetic field $\boldsymbol{E}(\boldsymbol{r},t)$ can be expanded in terms of normal modes $\boldsymbol{E}_n(\boldsymbol{r})$ with time-dependent complex amplitudes $a_n(t)$[15]. In open cavities a continuous spectrum of radiation modes is also present. The contributions of radiative and localized modes can be separated by a suitable projection onto two orthogonal subspaces [16, 17]. This leads to an effective theory on the subspace of localized modes in which they exchange a linear off-diagonal effective damping coupling. Radiation losses and gain are accounted for by additional linear terms (diagonal when the net gain is homogeneous), and the presence of a thermal bath is represented by the fluctuations due to the spontaneous emission. Nonlinear couplings arise from gain saturation and from the optical Kerr effect. At equilibrium with the pump mechanism, the complex amplitudes $a_n(t)$ are linked by a constraint given by the total optical intensity inside the system $\mathcal{E}=\epsilon N=\sum_{m=1}^{N}|a_m|^2$, where $N$ is the number of modes and $\epsilon$ the average energy per mode. The general Hamiltonian, derived by different approaches [9, 15, 18], reads

$$\mathcal{H}=-\Re\left[\frac{1}{2}\sum_{n_1,n_2}^{1,N}J_{\vec{n}_2}a_{n_1}a^*_{n_2}+\frac{1}{4!}\sum_{\omega_{n_1}+\omega_{n_3}=\omega_{n_2}+\omega_{n_4}}^{n_k=1,N}J_{\vec{n}_4}a_{n_1}a^*_{n_2}a_{n_3}a^*_{n_4}\right] \tag{1}$$

where $J_{\vec{n}_p}=J_{n_1\dots n_p}$ and the second sum ranges over all distinct 4-ples for which the so-called ML condition holds: $\omega_{n_1}-\omega_{n_2}+\omega_{n_3}-\omega_{n_4}=0$. The coupling coefficient $J_{\vec{n}_4}$ represents the spatial overlap of the electromagnetic

fields modulated by non-linear $\chi^{(3)}(\{\omega\};\boldsymbol{r})$ susceptibility:

$$J_{\vec{n}_4} = \frac{\imath}{2}\prod_{j=1}^{4}\sqrt{\omega_{n_j}}\int_V d^3r\ \chi^{(3)}_{\vec{\alpha}_4}(\{\omega_{\vec{n}_4}\};\mathbf{r}) \times E^{\alpha_1}_{n_1}(\mathbf{r})E^{\alpha_2}_{n_2}(\mathbf{r})E^{\alpha_3}_{n_3}(\mathbf{r})E^{\alpha_4}_{n_4}(\mathbf{r}) \quad (2)$$

with $\alpha_j = x, y, z$, and $\vec{n}_4 = \{n_1, n_2, n_3, n_4\}$. The linear coefficient $J_{\vec{n}_2}$ yields different contributions depending on medium randomness and cavity leakage:

$$J_{\vec{n}_2} = J_{n_1}\delta_{n_1 n_2} + J^{\rm rad}_{\vec{n}_2} + J^{\rm inh}_{\vec{n}_2} \quad (3)$$

$$J^{\rm inh}_{\vec{n}_2} = \frac{\imath}{2}\sqrt{\omega_{n_1}\omega_{n_2}}\int_V d^3r\ \chi^{(1)}_{\vec{\alpha}_2}(\mathbf{r})\ E^{\alpha_1}_{n_1}(\mathbf{r})E^{\alpha_2}_{n_2}(\mathbf{r}) \quad (4)$$

The linear diagonal terms of $J_{\vec{n}_2}$ depend on gain and loss profiles for the passive modes. A possible non-uniform distribution of the gain - and the related inhomogeneous linear susceptibility $\boldsymbol{\chi}^{(1)}(\boldsymbol{r})$ - yields the spatial overlap of localized eigenmodes, i. e., $J^{\rm inh}$, Eq. (4). Besides, in the *open cavity* scenario, the linear off-diagonal coupling terms also account for the presence of a continuous spectrum, and they correspond to the effective damping contribution $J^{\rm rad}$ obtained integrating out radiation modes [16, 17]. Taking the purely nonlinear interaction of a discrete set of modes corresponds to the *strong cavity limit*, $J^{\rm rad} = 0$, with homogeneous gain (because of orthogonality of $\{\boldsymbol{E}_n\}$'s it is $J^{\rm inh} = 0$). Only linear diagonal terms remain in this limit.

We build a mean-field theory in which the system is fully connected, that is, the network of interacting modes is a complete graph. This amounts to adopt a *narrow bandwidth* approximation for the gain profile in which $\omega_n \simeq \omega_0$, for each $n = 1, \ldots, N$ [41]. This is the case in the so-called *dispersive* RLs with very low finesse and a sensitive narrowing of the bandwidth above threshold, in which many modes oscillate in a relative small bandwidth and are so densely packed in frequency that their linewidths overlap. Consistently with this approximation we take a constant effective net gain profile in the bandwidth: $J_n = g(\omega_n) \simeq g(\omega_0) = g_0$, implying $\sum_{n_1,n_2} J_{\vec{n}_2} a_{n_1} a_{n_2} = g_0\mathcal{E} + \sum_{n_1\neq n_2} J_{\vec{n}_2} a_{n_1} a_{n_2}$.

The open cavity model in the narrow bandwidth approximation can be viewed as an extension of the so-called spherical 2+$p$ model [19–23] yielding a far reacher variety of physical scenarios.

The off-diagonal linear terms and the non-linear terms may, in general, be disordered because modes display different degree and shape of localizations [24, 25]. The constituents of the integrals in Eq. (2,4) are very difficult to calculate from first principles. The only specific form of the non-linear susceptibility has been computed by Lamb [26, 27] for few-modes standard lasers and no analogue study for RLs has been performed so far, to our knowledge. The overlap integrals in a disordered system can be regarded as a sum over many random variables. Correspondingly, the probability distribution of the couplings $J_{\vec{n}_p}$ can be assumed to be Gaussian:

$$P(J_{\vec{n}_p}) = \sqrt{\frac{N^{p-1}}{2\pi J_p^2}}\exp\left\{-\frac{N^{p-1}}{2J_p^2}\left[J_{\vec{n}_p} - \frac{J_0^{(p)}}{N^{p-1}}\right]^2\right\} \quad (5)$$

with $p = 2, 4$. To simplify the computation and its presentation we will take real-valued interaction couplings. This amounts, e. g., to neglect the effect of group velocity in the diagonal linear part and the Kerr lens effect in the nonlinear term, but does not change the generality of the qualitative picture. This is the most general Hamiltonian model for laser systems that one can consider. Indeed, also adding further non-linear terms ($J_{\vec{n}_p}$ with $p = 3, 5, 6, \ldots$) does not alter the qualitative behavior at the transition from continuous wave to (standard or random) lasing regimes.

*The external parameters* — In order to yield a comprehensive description, we introduce the *degrees of nonlinearity* $\alpha_0, \alpha$ - varying in the interval $[0, 1]$ - and suitable interaction energy scales $J_0, J$, for the ordered and disordered component, respectively:

$$J_0^{(4)} = \alpha_0 J_0;\ \ \alpha_0 = \left[\frac{J_0^{(2)}}{J_0^{(4)}} + 1\right]^{-1};\ \ J_0 = J_0^{(2)} + J_0^{(4)} \quad (6)$$

$$J_4 = \alpha J; \qquad \alpha = \left[\frac{J_2}{J_4} + 1\right]^{-1}; \quad J = J_2 + J_4 \quad (7)$$

The *degree of disorder* of a given system with coupling parameter scales $J, J_0$ is, then, defined as $R_J = J/J_0$.

The average energy per mode $\epsilon$ is related to the so-called *pumping rate* $\mathcal{P}$ induced by the pumping laser source in the RL, or proportional to the optical power in the cavity for the standard laser. In the present work it is defined as $\mathcal{P} \equiv \epsilon\sqrt{J_0/k_BT} = \epsilon\sqrt{\beta J_0}$ where $T$ is the heat-bath temperature. It encodes the experimental evidence that decreasing temperature [28] or increasing the total power [29] yields qualitatively similar behaviors. The factor $J_0$ is a material dependent parameter function of the angular frequency $\omega_0$ of the peak of the average spectrum, cf. Eq. (2), and it is volume independent.

To summarize, the parameters of interest are:

| | |
|---|---|
| Optical power per mode | $\epsilon$ |
| Heat-bath thermal energy | $k_BT = 1/\beta$ |
| Cumulative coupling average | $J_0 = J_0^{(2)} + J_0^{(4)}$ |
| Cumulative mean square disp. | $J = J_2 + J_4$ |
| Pumping rate | $\mathcal{P} = \epsilon\sqrt{\beta J_0}$ |
| Disorder degree | $R_J = J/J_0$ |
| Non-linearity degree (ordered) | $\alpha_0 = J_0^{(4)}/J_0$ |
| Non-linearity degree (disordered) | $\alpha = J_4/J$. |

We will consider here $\alpha = \alpha_0$ for simplicity, but cases with different degrees of non-linearity in ordered and disordered contributions can be also analyzed.

*Statistical mechanics with replicas.* — We study the model by means of the replica trick [30]. This enables to calculate the average free energy $f$ in the one step

Replica Symmetry Breaking (1RSB) Ansatz as a function of generalized order parameters, as detailed in the Appendix. We find a series of order parameters describing the physical regimes: (i) the intensity coherence of activated modes $m$; (ii) the phase coherence $r_d$; (iii-iv) the overlap parameters $q_{0,1}$ and (v) the RSB parameter $x$. The latter three specify degree and kind of glassiness. The free energy reads reads

$$\begin{aligned} 2\beta f(q_0,q_1,r_d,m) &= 2\beta f_0 + (1-x)w(q_1,q_1) \\ &+x\ w(q_0,q_0) - w(r_d,1) - 2k(m) - \ln(1-r_d) \\ &- \ln \mathcal{X}_1 - \frac{1}{x}\ln\frac{\mathcal{X}_0}{\mathcal{X}_1} - \frac{2q_0-m^2}{\mathcal{X}_0} \end{aligned} \tag{8}$$

with

$$\mathcal{X}_1 \equiv 1 + r_d - 2q_1\,; \quad \mathcal{X}_0 \equiv \mathcal{X}_1 + 2x(q_1-q_0) \tag{9}$$

$$w(t,u) \equiv \xi_2(t^2+u^2) + \frac{\xi_4}{2}(t^4+u^4+4t^2u^2) \tag{10}$$

$$k(m) \equiv k_2|m|^2 + k_4|m|^4 \tag{11}$$

$$\xi_2 = \frac{\beta^2\epsilon^2}{4}J_2^2\,; \qquad \xi_4 = \frac{\beta^2\epsilon^4}{6}J_4^2 \tag{12}$$

$$k_2 = \frac{\beta\epsilon}{4}J_0^{(2)}\,; \qquad k_4 = \frac{\beta\epsilon^2}{96}J_0^{(4)} \tag{13}$$

The self-consistency saddle point equations for the order parameters $m$, $r_d$, $q_{0,1}$, $x$ are given in the Appendix. These parameters determine all relevant thermodynamic phases (refer to Fig. 1):

∼ *Continuous wave regime* (CW). For small optical power, all modes oscillate independently in a CW incoherent noisy regime and the energy equally fluctuates among all passive modes. At low $\mathcal{P}$, for any degree of quenched disorder $R_J$ and non-linearity $\alpha$, all parameters are $q_{01} = m = r_d = 0$ ($x$ is irrelevant when $q_0 = q_1$).

♮ *Phase locking wave regime* (PLW). For non-zero disorder, increasing $\mathcal{P}$ the system undergoes a transition to a thermodynamic phase in which the mode phases lock on one given value, without stimulated amplification. Considering the complex amplitudes as continuous spherical spins in two dimensions, this corresponds to all spins pointing in the same direction though their intensity is freely oscillating. This phase has no counter-part in statistical mechanical models studied so far. The phase coherence parameter $r_d$ is non-zero, whereas $q_{0,1} = m = 0$. For increasing non-linearity $\alpha$, PLW occurs at lower and lower pumping rate $\mathcal{P}$.

‖ *Standard Mode-locking laser* (SML). For large $\mathcal{P}$ and $R_J = 0$ a localization transition occurs and the intensity is shared by activated modes, all of them oscillating coherently. This corresponds to standard passive ML laser systems [31], where a passive transition in $\mathcal{P}$ is predicted as a paramagnetic/ferromagnetic transition in Ref. [32] [42]. We further find that the CW/SML transition takes place also in presence of a limited amount of disorder $R_J \gtrsim 0$. The magnitude $m \neq 0$ in this regime so that light modes are coherent in intensity and stimulated amplification occurs.

⋆ *Random lasing* (RL). For high pumping rate and strong disorder, the tendency to oscillate synchronously is frustrated, resulting in a glassy phase representing the random laser regime. Modes are all coherent

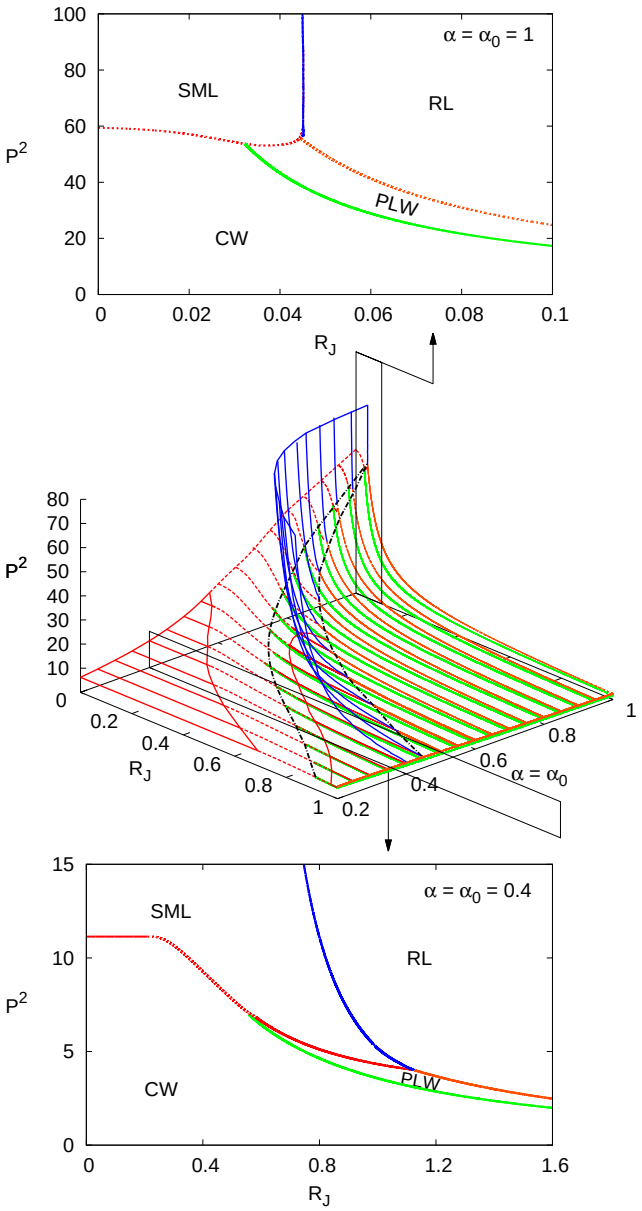


FIG. 1: Phase diagrams in the $(\mathcal{P}^2, R_J, \alpha = \alpha_0)$ space. For low disorder only the SML and CW phases occur varying pumping and degree of linearity. As disorder increases the intermediate PLW phase arise between CW and SML. For strong disorder RL replaces SML above the pumping threshold line. For any $R_J$, for low $\alpha_0$ the transition driven by $\mathcal{P}$ is continuous in the order parameters, whereas for high non-linearity ($\alpha > \alpha_{\rm nl} = 0.6297$) it is discontinuous. Insets: phase diagrams in the $(\mathcal{P}^2, R_J)$ plane for closed (right: $\alpha = \alpha_0 = 1$ and open ($\alpha = \alpha_0 = 0.4$) cavity.

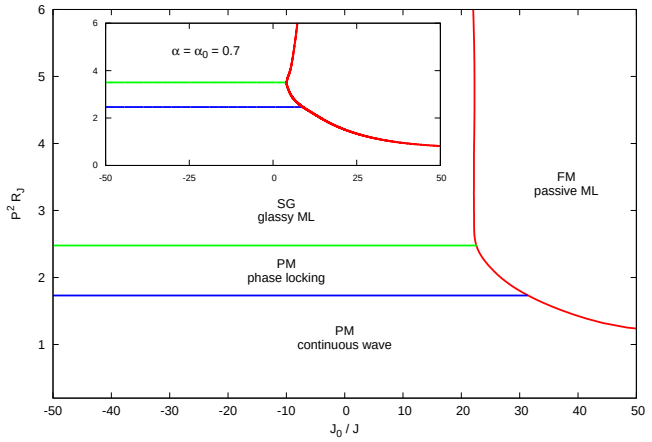


FIG. 2: Phase diagram in $\mathcal{P}^2 R_J = \beta\epsilon^2 J$ vs. $J_0/J = 1/R_J$ for closed cavity $\alpha = \alpha_0 = 1$ for $J_0/J$ ranging from negative to positive. Inset: open cavity with $\alpha = 0.7$.

in phase ($r_d \neq 0$) but not in intensity ($m = 0$), acquiring fixed random values. The thermodynamic phase is glassy with one step of RSB: $q_1 > q_0 = 0$ and $x \neq 0$ [43].

*Phase Diagram.* — In Fig. 1 we show the $\mathcal{P}^2$, $\alpha$, $R_J$ diagram in the main 3D plot. In the top inset the closed cavity projection for $\alpha = 1$ is displayed and in the bottom inset an open cavity instance, $\alpha = 0.4$.

For low degree of disorder $R_J$ there is a threshold between a CW (or PLW) phase and a SML; for large $R_J$ the threshold is to a RL. The CW/SML threshold line is plotted as solid (continuous transition) or dotted (discontinuous transition) dark (red) line and it occurs for $R_J \gtrsim 0$. The locus of tricritical (SML,CW,PWL) transition points is plotted as a black dashed-dotted line.

As $R_J$ is still small but a bit larger than the tricritical point, increasing the pumping one first has a CW/PWL transition denoted by a continuous light gray (green) line and then a PWL/SML. The latter can be continuous (solid dark-gray/red line) or discontinuous (dotted).

For larger $R_J$ we exclusively observe PWL/RL transition. The nature of the PWL/RL transition depends on the degree of non-linearity; it occurs both continuously, for $\alpha < \alpha_{\rm nl}$ or discontinuously, for $\alpha > \alpha_{\rm nl}$, see Appendix. In Fig. 1 it is $\alpha_{\rm nl} = 0.6297$.

Supposing, further, that in an optically active material the degree of disorder $R_J$ could be continuously changed, the phase diagram also predicts a transition between SML and RL for pumping above threshold, represented by the nearly vertical solid (blue) transition lines. The locus of the tricritical points RL/SML/PWL is plotted as a second black dashed-dotted line in the main plot.

*Mode locking without saturable absorber* — A key point in the present study is that the transition from continuous wave to standard passive mode-locking (CW→ SML) only occurs for a strictly positive value of the coupling coefficient $J_0$, as shown in Figs. (1,2). This formally corresponds to the presence of a saturable absorber in the cavity [15]. In RLs such a device is not present, and, hence, the occurrence of this lasing transition is not to be given for granted. However, in Fig. (1) it is shown that starting from a standard laser supporting passive mode-locking and increasing the disorder, the CW/SML transition acquires the character of a glassy mode-locking CW/RL transition. This is present also for $J_0 < 0$, as explicitly shown in Fig. (2). It is far from trivial that the latter mode-locking transition, ruled out for ordered lasers without a saturable absorber ($J_0 \ll J$), spontaneously occurs as an effect of the quenched disorder, i.e., for large enough $R_J$. The physical origin is the mode coupling due to the open cavity configuration.

*Conclusions* — We developed a theory for light wave systems in optically active random media with narrow bandwidth and in which all activated mode localization spatially overlap with each other. The theory is based on the most general Hamiltonian for an open system, including non-linearity and coupling to a thermal bath that measures the amount of energy transferred to the system by an external pumping system at equilibrium. This corresponds to a mean-field fully connected disordered system in statistical mechanics. We derive the most general phase diagram, ranging from closed cavities that correspond to a standard laser, to completely open cavities, representing the random lasers. The resulting picture, given in terms of order parameters that represent the correlations among amplitudes, phases, and their cross correlation, furnishes a number of different equilibrium phases affected by non-linearity and disorder. These include standard passive-mode locking in standard lasers, and different coherent regimes attainable in random lasers. The reported results open the way to further investigations, as the study of open quantum systems, testing theoretical models for the statistical mechanics of disordered systems, employing variable coherence sources for applications in spectroscopy and microscopy, and developing novel techniques for mode locking and ultrashort pulse generation not requiring saturable absorbers.

*Acknowledgments* — The research leading to these results has received funding from the People Programme (Marie Curie Actions) of the European Union's Seventh Framework Programme FP7/2007-2013/ under REA grant agreement n 290038, NETADIS project, from the European Research Council through ERC grant agreement no. 247328 - CriPheRaSy project - and from the Italian MIUR under the Basic Research Investigation Fund FIRB2008 program, grant No. RBFR08M3P4, and under the PRIN2010 program, grant code 2010HXAW77-008.

### Appendix: Replica Calculations

In this appendix we carry out explicit replica calculations first in the general framework and then in the specific one step Replica Symmetry Breaking (RSB) Ansatz. In the following, we show the complete derivation of the free energy functional and the self-consistency equations for the relevant order parameters describing the regimes reported in the paper.

In our *narrow bandwidth* approximation, given a line-width $\delta\omega$ any frequency difference $|\omega_i - \omega_j| \ll \delta\omega$. In other words the band-width $\Delta\omega$ of the spectrum of the optically active medium is comparable with, or less than, the line-width of each mode and the system finesse is $f \equiv \Delta\omega/\delta\omega < 1$.

The diagonal part of the pairwise interaction of Eq. (3), with real $J$'s, represents the net gain frequency profile

$$J_n = g(\omega_n) \ .$$

In this narrow-band approximation the corresponding contribution to the Hamiltonian becomes:

$$-\frac{1}{2}\sum_n J_n |a_n|^2 = -\frac{1}{2} g(\omega_0)\epsilon N \tag{14}$$

that is, an irrelevant constant in the dynamics.

Naming real and imaginary part of the complex amplitudes as

$$a = \sigma + \imath\tau$$

and neglecting the diagonal term, Eq. (14), the Hamiltonian - Eq. 1 of the main text - becomes

$$\begin{aligned} \mathcal{H} \ = \ & -\sum_{n_1<n_2} J_{n_1 n_2}(\sigma_{\vec{n}_2} + \tau_{\vec{n}_2}) \\ & -\sum_{n_1<n_2<n_3<n_4} J_{n_1 n_2 n_3 n_4}(\sigma_{\vec{n}_4} + \tau_{\vec{n}_4} + \Theta_{\vec{n}_4}) \end{aligned} \tag{15}$$

with

$$\begin{aligned} \Theta_{\vec{n}_4} \ &\equiv \ \frac{1}{3}\left(\psi_{n_1 n_2, n_3 n_4} + \psi_{n_1 n_3, n_2 n_4} + \psi_{n_1 n_4, n_2 n_3}\right) \ , \\ \psi_{n_1 n_2, n_3 n_4} \ &\equiv \ \sigma_{n_1 n_2}\tau_{n_3 n_4} + \sigma_{n_3 n_4}\tau_{n_1 n_2} \ , \\ \sigma_{n_x n_y} \ &= \ \sigma_{n_x}\sigma_{n_y} \qquad ; \qquad \sigma_{\vec{n}_p} \ = \ \prod_{j=1}^{p}\sigma_{n_j} \ . \end{aligned}$$

In a nutshell, we study the model thermodynamics by means of the replica trick [30]:

$$\begin{aligned} \langle \ln Z[J]\rangle_{P(J)} &= \lim_{n\to 0}\frac{1}{n}\left[\langle Z^n[J]\rangle_{P(J)} - 1\right] \\ Z^n[J] &= \sum_{\{\{a^{(1)}\},\ldots,\{a^{(n)}\}\}} \exp\left\{-\beta\sum_{\nu=1}^{n}\mathcal{H}[\{a^{(\nu)}\}|\{J\}]\right\} \end{aligned}$$

where $\{a^{(\nu)}\} = \sigma^\nu + \imath\tau^\nu$ is the mode amplitude configuration in the replica $\nu$. The random interaction network is copied $n$ times, the partition function is computed for $n$ copies and, eventually, the analytic continuation to real $n$ is computed in the $n \to 0$ limit, yielding the expression for the average free energy

$$\beta f(\mathcal{Q}) = -\frac{1}{N}\langle \ln Z[J]\rangle_{P(J)}\big|_{S.P.} \tag{16}$$

as a function of a given saddle point solution for the set of order parameters $\mathcal{Q}$.

Rescaling the degrees of freedom as

$$\sigma \to \sqrt{\frac{\epsilon}{2}}\,\sigma \quad ; \quad \tau \to \sqrt{\frac{\epsilon}{2}}\,\tau \ ,$$

the average over the $J$'s distribution of the partition function of the spherical model replicated $n$ times turns out to be

$$\begin{aligned} \langle Z^n[J]\rangle_{P(J)} \ = & \int_{\mathcal{S}_n}\mathcal{D}\sigma\ \mathcal{D}\tau\ \exp\Bigg\{\frac{2k_2}{N}\sum_{n_1<n_2}\sum_{a=1}^{n}\left(\sigma^a_{\vec{n}_2} + \tau^a_{\vec{n}_2}\right) \\ & + \frac{\xi_2}{2N}\sum_{n_1<n_2}\sum_{ab}\left(\sigma^a_{\vec{n}_2} + \tau^a_{\vec{n}_2}\right)\left(\sigma^b_{\vec{n}_2} + \tau^b_{\vec{n}_2}\right) \\ & + \frac{24k_4}{N^3}\sum_{n_1<n_2<n_3<n_4}\sum_{a=1}^{n}\left(\sigma^a_{\vec{n}_4} + \tau^a_{\vec{n}_4} + \Theta^a_{\vec{n}_4}\right) \\ & + \frac{9\xi_4}{4N^3}\sum_{n_1<n_2<n_3<n_4}\sum_{ab}\left(\sigma^a_{\vec{n}_4} + \tau^a_{\vec{n}_4} + \Theta^a_{\vec{n}_4}\right) \\ & \times\left(\sigma^b_{\vec{n}_4} + \tau^b_{\vec{n}_4} + \Theta^b_{\vec{n}_4}\right)\Bigg\} \end{aligned} \tag{17}$$

with

$$\mathcal{D}\sigma = \prod_{i=1}^{N}\prod_{a=1}^{n} d\sigma_i^{(a)} \ ,$$

and where the integral is over the $n$ hyper-spheres $\mathcal{S}_N$ given by the spherical constraint

$$\sum_{i=1}^{N}\left(\sigma_i^{(a)} + \tau_i^{(a)}\right)^2 = 2N. \tag{18}$$

The average pump energy per mode $\epsilon$ now enters only in the parameters $\xi_2$, $\xi_4$, $k_2$ and $k_4$ as defined in Eqs. (12-13) of the main text.

Introducing as in the following the overlap parameters between replicas

$$Q_{ab} = \frac{1}{2N}\sum_{j=1}^{N}\left(\sigma_j^a\sigma_j^b + \tau_j^a\tau_j^b\right) \quad (19)$$

$$R_{ab} = \frac{1}{2N}\sum_{j=1}^{N}\left(\sigma_j^a\sigma_j^b - \tau_j^a\tau_j^b\right) \quad (20)$$

$$T_{ab} = \frac{1}{N}\sum_{j=1}^{N}\sigma_j^a\tau_j^b \quad (21)$$

and the magnetization vectors in the replica space (the super-index $R$ stands for real, $I$ stand for imaginary)

$$m_a^R = \frac{1}{N}\sum_{j=1}^{N}\sigma_j^a \quad (22)$$

$$m_a^I = \frac{1}{N}\sum_{j=1}^{N}\tau_j^a \ , \quad (23)$$

with further manipulations we sum in the partition function over the configurations of real and imaginary parts of the complex amplitudes, ending up with the replicated free energy and the saddle point equations for the order parameters.

Before reporting the calculation, though, we observe that, for symmetry reasons, in absence of an external field linearly coupled to $\sigma$ or to $\tau$ or, more generally, coupled to any simple function of the phase of the complex amplitude $\phi = \arctan(\tau/\sigma)$, it holds

$$T_{ab} = T_{ba} = 0; \qquad \forall a, b \qquad . \quad (24)$$

Generalizing a well known procedure for $p$-spin models [33, 34], the above defined parameters Eqs. (19), (20), (22) and (23) are inserted in Eq. (17) as Dirac deltas and these are expressed in their Fourier form, introducing further parameters, the Lagrange multipliers $\lambda_{ab}$, $\mu_{ab}$, $\kappa_a^R$, $\kappa_a^I$

Carrying out this approach we end up with

$$\langle Z^n[J]\rangle_{P(J)} = \int \mathcal{D}\boldsymbol{Q}\ \mathcal{D}\boldsymbol{\lambda}\exp\Big\{-NG(\boldsymbol{Q},\boldsymbol{\lambda})\Big\} \quad (25)$$

with $\boldsymbol{Q} = \{Q, R, \boldsymbol{m}\}$ and $\boldsymbol{\lambda} = \{\lambda, \mu, \boldsymbol{\kappa}\}$, and where we introduce the $2n$ column vectors

$$\boldsymbol{m} \equiv \left(m_1^R, \ldots, m_n^R, m_1^I, \ldots, m_n^I\right)^T$$
$$\boldsymbol{\kappa} \equiv \left(\kappa_1^R, \ldots, \kappa_n^R, \kappa_1^I, \ldots, \kappa_n^I\right)^T$$

to shorten the notation. The replicated free energy functional, then, reads

$$G(\boldsymbol{Q},\boldsymbol{\lambda}) \equiv A(\boldsymbol{Q}) + B(\boldsymbol{Q},\boldsymbol{\lambda}) - \ln\mathcal{Z}(\boldsymbol{\lambda}) \quad (26)$$

$$A(\boldsymbol{Q}) \equiv -\frac{\xi_2}{2}\sum_{ab}\left(Q_{ab}^2 + R_{ab}^2\right) \quad (27)$$
$$-\frac{\xi_4}{4}\sum_{ab}\left(Q_{ab}^4 + R_{ab}^4 + 4Q_{ab}^2R_{ab}^2\right)$$
$$-k_2\ \boldsymbol{m}^T\cdot\boldsymbol{m} - k_4\ \left[\boldsymbol{m}^T\cdot\boldsymbol{m}\right]^2$$

$$B(\boldsymbol{Q},\boldsymbol{\lambda}) = \sum_{ab}\left(\lambda_{ab}Q_{ab} + \mu_{ab}R_{ab}\right) + \boldsymbol{\kappa}^T\cdot\boldsymbol{m} \quad (28)$$

$$\mathcal{Z}(\boldsymbol{\lambda}) = \int \mathcal{D}\sigma\,\mathcal{D}\tau\,\exp\Big\{\sum_a\left(\kappa_a^R\sigma_a + \kappa_a^I\tau_a\right) \quad (29)$$
$$+\frac{1}{2}\sum_{ab}\left[\sigma_a(\lambda_{ab}+\mu_{ab})\sigma_b + \tau_a(\lambda_{ab}-\mu_{ab})\tau_b\right]\Big\}$$
$$= \frac{(2\pi)^n}{\sqrt{\det(-\lambda-\mu)\det(-\lambda+\mu)}}$$
$$\times\exp\Big\{-\frac{1}{2}(\boldsymbol{\kappa}^R)^T(\lambda+\mu)^{-1}\boldsymbol{\kappa}^R$$
$$-\frac{1}{2}(\boldsymbol{\kappa}^I)^T(\lambda-\mu)^{-1}\boldsymbol{\kappa}^I\Big\}$$

The latter term in Eq. (26) can be written as

$$-\ln\mathcal{Z}(\boldsymbol{\lambda}) = \frac{1}{2}\ln\det W - \frac{1}{2}\boldsymbol{\kappa}^T W^{-1}\boldsymbol{\kappa} \quad (30)$$

$$W \equiv -\begin{pmatrix}\lambda+\mu & 0\\ 0 & \lambda-\mu\end{pmatrix} \quad (31)$$

Saddle point equations $\partial G/\partial\boldsymbol{\lambda} = 0$ obtained deriving with respect to $\lambda_{ab}$, $\mu_{ab}$, and $\kappa_a$, turn out to be, respectively

$$2Q - \boldsymbol{m}^R\boldsymbol{m}^R - \boldsymbol{m}^I\boldsymbol{m}^I = -(\lambda+\mu)^{-1} - (\lambda-\mu)^{-1}$$
$$2R - \boldsymbol{m}^R\boldsymbol{m}^R + \boldsymbol{m}^I\boldsymbol{m}^I = -(\lambda+\mu)^{-1} + (\lambda-\mu)^{-1}$$
$$\boldsymbol{m} = W^{-1}\boldsymbol{\kappa}$$

yielding the self-consistency relations

$$\lambda+\mu = -\left(Q + R - \boldsymbol{m}^R\boldsymbol{m}^R\right)^{-1} \quad (32)$$
$$\lambda-\mu = -\left(Q - R - \boldsymbol{m}^I\boldsymbol{m}^I\right)^{-1} \quad (33)$$
$$\boldsymbol{\kappa}^{R,I} = \left(Q + R - \boldsymbol{m}^{R,I}\boldsymbol{m}^{R,I}\right)^{-1}\boldsymbol{m}^{R,I} \quad (34)$$

Using Eqs. (32-34) and observing that of Eq. (28) plus the last term in Eq. (30) sum up to zero, that is,

$$B(\boldsymbol{Q},\boldsymbol{\lambda}) - \frac{1}{2}\boldsymbol{\kappa}^T W^{-1}\boldsymbol{\kappa}$$
$$= \sum_{ab}\left(\lambda_{ab}Q_{ab} + \mu_{ab}R_{ab}\right) + \frac{1}{2}\boldsymbol{\kappa}^T\cdot\boldsymbol{m} = 0 \ ,$$

The subsequent saddle point equations from stationarity of $G(\boldsymbol{Q})$ with respect to the elements of $Q, R$ and $\boldsymbol{m}$

are

$$2\xi_2 Q_{ab} + 2\xi_4 \left(Q_{ab}^3 + 2Q_{ab}R_{ab}^2\right) \quad (35)$$
$$= -(Q + R - \boldsymbol{m}^R\boldsymbol{m}^R)^{-1}_{ab} - (Q - R - \boldsymbol{m}^I\boldsymbol{m}^I)^{-1}_{ab}$$
$$2\xi_2 R_{ab} + 2\xi_4 \left(R_{ab}^3 + 2R_{ab}Q_{ab}^2\right) \quad (36)$$
$$= -(Q + R - \boldsymbol{m}^R\boldsymbol{m}^R)^{-1}_{ab} + (Q - R - \boldsymbol{m}^I\boldsymbol{m}^I)^{-1}_{ab}$$
$$2k_2 m_a^R + 4k_4 \left[(m_a^R)^3 + m_a^R (m_a^I)^2\right] \quad (37)$$
$$= \left[\boldsymbol{m}^R (Q + R - \boldsymbol{m}^R\boldsymbol{m}^R)^{-1}\right]_a$$
$$2k_2 m_a^I + 4k_4 \left[(m_a^I)^3 + m_a^I (m^I R_a)^2\right] \quad (38)$$
$$= \left[\boldsymbol{m}^I (Q - R - \boldsymbol{m}^I\boldsymbol{m}^I)^{-1}\right]_a$$

Using Eqs. (35-38), Eqs. (32-34) lead to

$$\lambda_{ab} = \xi_2 Q_{ab} + \xi_4 Q_{ab}\left(Q_{ab}^2 + 2R_{ab}^2\right) \quad (39)$$
$$\mu_{ab} = \xi_2 R_{ab} + \xi_4 R_{ab}\left(R_{ab}^2 + 2Q_{ab}^2\right) \quad (40)$$
$$\boldsymbol{\kappa} = 2k_2\boldsymbol{m} + 4k_4\boldsymbol{m}(\boldsymbol{m}^T\cdot\boldsymbol{m}) \quad (41)$$

Eventually, using that

$$\ln\det(Q \pm R - \boldsymbol{m}^{R,I}\boldsymbol{m}^{R,I}) = \quad (42)$$
$$= \ln\det(Q \pm R) - (\boldsymbol{m}^{R,I})^T (Q \pm R)^{-1}\boldsymbol{m}^{R,I} + O(n^2)$$

we write the free energy Eq. (26) in the form

$$G(\boldsymbol{Q}) = -\frac{1}{2}\sum_{ab} w(Q_{ab}, R_{ab}) - \sum_a k(\boldsymbol{m}_a) \quad (43)$$
$$-\frac{1}{2}\ln\det(Q + R) - \frac{1}{2}\ln\det(Q - R)$$
$$-n\ln\frac{\epsilon}{2} + \frac{1}{2}(\boldsymbol{m}^R)^T (Q + R)^{-1}\boldsymbol{m}^R$$
$$+\frac{1}{2}(\boldsymbol{m}^I)^T (Q - R)^{-1}\boldsymbol{m}^I$$

with, cf. Eqs. (10-11) of the main text,

$$w(t,u) \equiv \xi_2(t^2 + u^2) + \frac{\xi_4}{2}(t^4 + u^4 + 4t^2u^2)$$
$$k(\boldsymbol{m}) \equiv k_2\ \boldsymbol{m}^T\cdot\boldsymbol{m} + k_4(\boldsymbol{m}^T\cdot\boldsymbol{m})^2\,.$$

The diagonal parts will now be $Q_{aa} = 1$, because of the complex spherical constraint, cf. Eqs. (18,19), and we will, further, term $R_{aa} = r_d$.

The stationarity equations take the form

$$\Lambda(Q_{ab}, R_{ab}) + |\boldsymbol{m}|^2 B(\boldsymbol{m}) = \quad (44)$$
$$= -(Q + R)^{-1}_{ab} - (Q - R)^{-1}_{ab}$$
$$\Lambda(R_{ab}, Q_{ab}) + \left[(m^R)^2 - (m^I)^2\right] B(\boldsymbol{m}) \quad (45)$$
$$= -(Q + R)^{-1}_{ab} + (Q - R)^{-1}_{ab}$$
$$m^{R,I} B(\boldsymbol{m}) = m^{R,I}\sum_b (Q \pm R)^{-1}_{ab} \quad (46)$$

where

$$\Lambda(t,u) \equiv 2t[\xi_2 + \xi_4(t^2 + 2u^2)]$$
$$B(\boldsymbol{m}) \equiv 2k_2 + 4k_4|\boldsymbol{m}|^2$$

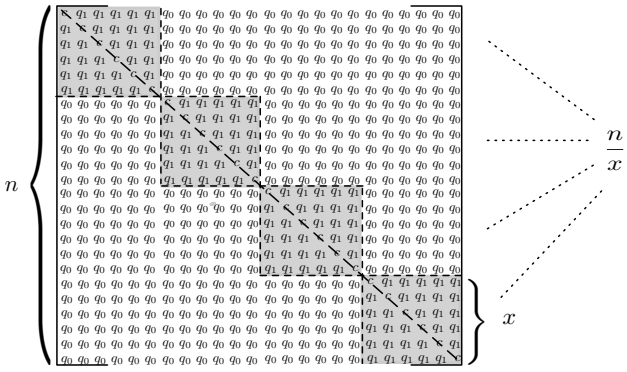


FIG. 3: 1RSB scheme for the elements of the $Q_{ab}$ overlap parameter matrix. As $n \to 0$, $x$ becomes a continuous variable in the intervall $[0:1]$. The elements of $Q_{ab}$ acquire two values: $q_0$, if in an off-diagonal block, and $q_1 > q_0$ inside the diagonal blocks (diagonal excluded).

We have dropped the replica dependence of $\boldsymbol{m}^T = (m^R, m^I)$ since observables depending on single replica index do not break replica symmetry [35] and the sum along each row/column of any function of the $\boldsymbol{Q}$ matrices is invariant under column/row permutation.

We now notice that any solution to the above equations (46) implies

$$m^R m^I = 0 \quad (47)$$

and this is a consequence of Eq. (24). Choosing, then, without loss of generality, $m^I = 0$, Eqs. (44-46) are solved by

$$R_{ab} = Q_{ab} \qquad a \neq b \quad (48)$$

For the diagonal part still holds $Q_{aa} = 1$, $R_{aa} = r_d$.

*Replica Symmetry Breaking* — We will not show here the stability analysis of the various Replica Symmetry Breaking Ansätze involved in given regions of the phase diagram. Even though the most general stable solution to the problem is within a Full RSB scheme [36], that is a *continuous* overlap function $q(x)$ in the interval $x \in [0,1]$, for the sake of clarity in the presentation, and without loss of generality for what concerns the study of the threshold behaviors, we will adopt the one step RSB scheme, cf. Fig. 3. Calling, as in the figure, $x$ the number of elements in a row of a diagonal block of $Q_{ab}$, the elements take two values according to the rule

$$Q_{ab} = \begin{cases} q_1 & \text{if } N(a/x) = N(b/x) \\ q_0 & \text{if } N(a/x) \neq N(b/x) \end{cases} \quad (49)$$

being $N(a/x)$ the integer part of $a/x$.

In this Ansatz the free energy take the form shown in Eq. (8) of the main text, where the self-consistency saddle point equations for the order parameters $m$, $r_d$, $q_{0,1}$, $x$ are given by

$$m\ B(m) = \frac{m}{\mathcal{X}_0} \tag{50}$$

$$\Lambda(q_0,q_0)+m^2B^2(m) = \frac{2q_0}{\mathcal{X}_0} \tag{51}$$

$$\Lambda(q_1,q_1)-\Lambda(q_0,q_0) = \frac{2(q_1-q_0)}{\mathcal{X}_0\mathcal{X}_1} \tag{52}$$

$$\Lambda(r_d,1)-\Lambda(q_1,q_1) = \frac{1}{1-r_d}-\frac{1}{\mathcal{X}_1} \tag{53}$$

$$w(q_1,q_1)-w(q_0,q_0) = \frac{1}{x^2}\ln\frac{\mathcal{X}_0}{\mathcal{X}_1}-\frac{2(q_1-q_0)}{x\mathcal{X}_0} + \frac{2(q_1-q_0)(2q_0-m^2)}{\mathcal{X}_0^2} \tag{54}$$

where the last equation corresponds to the stationarity in the $x$ parameter [44]. These are the parameters that describe all relevant thermodynamic phases involved, as displayed in Fig. 1 of the main text.

For $\alpha > \alpha_{\rm nl} \simeq (3-1.76382\epsilon)(3-1.03703\epsilon^2)^{-1}$ ($\simeq 0.6297$ for $\epsilon=1$), that is both for open and closed cavity, the 1RSB solution is stable above pumping threshold and it reduces discontinuously to an RS solution below threshold. This is the exact solution. For small $\alpha < \alpha_{\rm nl}$, that is, for extremely open cavities, instead, the actual solution is Full RSB and it reduces continuously to a Replica Symmetric solution below threshold ($q_1-q_0\to 0$). In virtue of this continuity at the transition, the 1RSB solution very well qualitatively and quantitatively approximates the Full RSB solution next to the PWL/RL transition line.

We postpone to a more technical paper the complete description of the complex amplitude model with fixed optical power in terms of replica symmetry breaking solutions and their stability analysis [45].

* Electronic address: luca.leuzzi@cnr.it


[1] V. S. Lethokov, Sov. Phys. JETP **26**, 835 (1968).
[2] N. M. Lawandy, R. M. Balachandran, A. S. L. Gomes, and E. Sauvain, Nature **368**, 436 (1994).
[3] H. Cao, Y. G. Zhao, S. T. Ho, E. W. Seelig, Q. H. Wang, and R. P. H. Chang, Phys. Rev. Lett. **82**, 2278 (1999).
[4] P. Sebbah and C. Vanneste, Phys. Rev. B **66**, 144202 (2002).
[5] H. Cao, J. Phys. A. : Math. Gen. **38**, 10497 (2005).
[6] H. E. Tureci, A. D. Stone, and B. Collier, Phys. Rev. A **74**, 043822 (2006).
[7] H. E. Tureci, L. Ge, S. Rotter, and A. D. Stone, Science **320**, 643 (2008).
[8] D. S. Wiersma, Nature Physics **4**, 359 (2008).
[9] L. Leuzzi, C. Conti, V. Folli, L. Angelani, and G. Ruocco, Phys. Rev. Lett. **102**, 083901 (2009).
[10] S. K. Turitsyn, S. A. Babin, A. E. El-Taher, P. Harper, D. V. Churkin, S. I. Kablukov, J. D. Ania-Castanon, V. Karalekas, and E. V. Podivilov, Nat Photon **4**, 231 (2010).
[11] O. Zaitsev and L. Deych, J. Opt. **12**, 024001 (2010).
[12] M. Leonetti, C. Conti, and C. Lopez, Nature Comm. **4**, 1740 (2013).
[13] M. Leonetti and C. Lopez, Appl. Phys. Lett. **102**, 071105 (2013).
[14] M. Leonetti, C. Conti, and C. Lopez, Light Sci. Appl. **2**, 88 (2013).
[15] C. Conti and L. Leuzzi, Phys. Rev. B **83**, 134204 (2011).
[16] G. Hackenbroich, C. Viviescas, and F. Haake, Phys. Rev. A **68**, 063805 (2003).
[17] C. Viviescas and G. Hackenbroich, Phys. Rev. A **67**, 013805 (2003).
[18] L. Angelani, C. Conti, G. Ruocco, and F. Zamponi, Phys. Rev. B **74**, 104207 (2006).
[19] T. M. Nieuwenhuizen, Phys. Rev. Lett. **74**, 4289 (1995).
[20] A. Crisanti and L. Leuzzi, Phys. Rev. Lett. **93**, 217203 (2004).
[21] A. Crisanti and L. Leuzzi, Phys. Rev. B **73**, 014412 (2006).
[22] A. Crisanti and L. Leuzzi, Phys. Rev. B **75**, 144301 (2007).
[23] A. Crisanti and L. Leuzzi, Nucl. Phys. B **870**, 176 (2013).
[24] C. Conti and A. Fratalocchi, Nat. Physics **4**, 794 (2008).
[25] J. Fallert, R. J. B. Dietz, J. Sartor, D. Schneider, C. Klingshirn, and H. Kalt, Nat. Photon. **3**, 279 (2009).
[26] W. E. Lamb, Phys. Rev. **134**, A1429 (1964).
[27] Murray Sargent III, Marlan O'Scully and Willis E. Lamb, *Laser Physics* (Addison Wesley Publishing Company, 1978).
[28] D. S. Wiersma and S. Cavalieri, Nature **414**, 708 (2001).
[29] M. Leonetti and C. Conti, J. Opt. Soc. Am. **27**, 1446 (2010).
[30] S. Edwards and P. Anderson, J. Phys. F **5**, 965 (1975).
[31] H. A. Haus, IEEE J. Quantum Electron. **6**, 1173 (2000).
[32] A. Gordon and B. Fischer, Opt. Comm. **223**, 151 (2003).
[33] E. Gardner, Nucl. Phys. B **257**, 747 (1985).
[34] A. Crisanti and H.-J. Sommers, Zeit. Phys. B **87**, 341 (1992).
[35] A. Crisanti and L. Leuzzi, Phys. Rev. B **70**, 014409 (2004).
[36] G. Parisi, J. Phys. A **13**, L115 (1980).
[37] C. Weiss and R. Vilaseca, *Dynamics of lasers* (VCH, Weinheim (Germany], 1991).
[38] A. Crisanti, M. Falcioni, and A. Vulpiani, Phys. Rev. Lett. **76**, 612 (1996).
[39] P. Meystre and M. Sargent III, *Elements of Quantum Optics* (Springer, 1998).
[40] We stress that by non-deterministic we do not mean chaotic, since chaos is, actually, deterministic. Chaos is an apart dynamic phenomenon occurring in laser systems, [37] but it does not, actually, affect the presence or absence of glassiness, as, e.g., shown in Ref. [38]. Chaos is not a necessary feature for RLs, nor it is sufficient one.
[41] More specifically, $|\omega_j-\omega_k|<\delta\omega$, for each $j,k=1,\ldots,N$, where $\delta\omega$ is the line-width of the intensity spectrum. Indeed, in most of RLs, it is not necessary that the resonant ML condition for having four modes interact is satisfied exactly [39].
[42] The $R_J=0$ limit of our theory confirms previous estimates. To quantitatively compare we have rescaled our

parameters in the notation of Ref. [32], where the transition point was given in the parameter $T/\gamma_s P_0^2 = 8/\mathcal{P}^2$, with $P_0 = \epsilon$ and $\gamma_s = J_0/8$. In the quenched amplitude approximation we have $8/\mathcal{P}^2 = 0.1828$ and in the free amplitude model we find $8/\mathcal{P}^2 = 0.1357$, both compatible with previous results.

[43] This is strictly true in the whole glassy light phase above threshold when non-linearity is dominating and the transition is discontinuous in the order parameters, see Appendix. In systems where $\alpha$ is small, instead, a glassy phase is still present but it is of a different nature and, actually, described by an infinite step RSB. Since, though, this "linearly runned" transition is continuous in the overlap, rather than discontinuous as for $\alpha > \alpha_{\rm nl}$, the 1RSB is a fully justified approximation next to the lasing where $q_1 \gtrsim q_0 \gtrsim 0$.

[44] We name the integer number of elements in a diagonal block in Fig. 3 and its analytic continuation in the $n \to 0$ limit invariably by $x$.

[45] For what concerns the purely real $2 + 4$ spherical spin model the reader can refer to [20, 21, 23].